Magnetic Anisotropy of $[Mo(CN)_7]^{4-}$ Anions and Fragments of Cyano-Bridged Magnetic Networks

Liviu F. Chibotaru,*,† Marc F. A. Hendrickx,† Sergiu Clima,† Joulia Larionova,‡ and Arnout Ceulemans†

Laboratorium voor Kwantumchemie, Katholieke Universiteit Leuven, Celestijnenlaan 200F, B-3001 Belgium, and Laboratoire de Chimie Moléculaire et Organization du Solide, UMR 5637, Université Montpellier II, Place E. Bataillon, 34095 Montpellier Cedex 5, France

Received: April 11, 2005; In Final Form: June 7, 2005

Quantum chemistry calculations of CASSCF/CASPT2 level together with ligand field analysis are used for the investigation of magnetic anisotropy of $[Mo(CN)_7]^{4-}$ complexes. We have considered three types of heptacyano environments: two ideal geometries, a pentagonal bipyramid and a capped trigonal prism, and the heptacyanomolybdate fragment of the cyano-bridged magnetic network $K_2[Mn(H_2O)_2]_3[Mo(CN)_7]_2\cdot 6H_2O$. At all geometries the first excited Kramers doublet is found remarkably close to the ground one due to a small orbital energy gap in the ligand field spectrum, which ranges between a maximal value in the capped trigonal prism (800 cm^{-1}) and zero in the pentagonal bipyramid. The small value of this gap explains (i) the axial form of the g tensor and (ii) the strong magnetic anisotropy even in strongly distorted complexes. Comparison with available experimental data for the g tensor of the mononuclear precursors reveals good agreement with the present calculations for the capped trigonal prismatic complex and a significant discrepancy for the pentagonal bipyramidal one. The calculations for the heptacyanomolybdate fragment of $K_2[Mn(H_2O)_2]_3$-$[Mo(CN)_7]_2\cdot 6H_2O$ give $g_\perp/g_\parallel \approx 0.5$ and the orientation of the local anisotropy axis close to the symmetry axis of an idealized pentagonal bipyramid. These findings are expected to be important for the understanding of the magnetism of anisotropic Mo(III)−Mn(II) cyano-bridged networks based on the $[Mo(CN)_7]^{4-}$ building block.

Introduction

Currently there is a revival of interest in the investigation of magnetic anisotropy of molecular magnets, mainly as a result of its capability to create barriers for reversal of magnetization in polynuclear complexes resulting in the phenomenon of single-molecule magnets.[1] On the theoretical side, the understanding of the mechanisms allowing control of the magnetic anisotropy of monomer molecules and clusters becomes therefore increasingly important.[2] The important sources of magnetic anisotropy in polynuclear complexes are the single-ion anisotropy of magnetic sites and the anisotropy of intersite exchange interactions.[3−5] Both these contributions are determined by the effects of spin−orbit coupling in the ground state of individual metal sites, which are generally quite sensitive to the geometry of the corresponding coordination environments. Of particular interest in this respect is the heptacyanomolybdate complex $[Mo(CN)_7]^{4-}$, which exhibits significant magnetic anisotropy for different geometries of the cyanide environment.

Five geometries exist for seven-coordinated metal ion, the pentagonal bipyramid (D_{5h}), capped trigonal prism (C_{2v}), monocapped octahedron (C_{3v}), heptagon (D_{7h}), and hexagonal pyramid (C_{6v}). $[Mo(CN)_7]^{4-}$ is known to adopt two major geometries in the precursor form: pentagonal bipyramid and capped trigonal prism. In the investigated complexes, such as $K_5[Mo(CN)_7]\cdot H_2O$, $K_4[Mo(CN)_7]\cdot 2H_2O$ (and the aqueous solution),[6] $Na_5[Mo(CN)_7]\cdot 10H_2O$,[7] or the mixed salt $NaK_3[Mo(CN)_7]\cdot 2H_2O$,[8] it has a pentagonal bipyramidal structure. However, in the solid state, the anion of $K_4[Mo(CN)_7]\cdot 2H_2O$ adopts a capped trigonal prismatic structure.[6]

Recently, a new class of molecular magnetic materials, Mo(III)−Mn(II) cyano-bridged networks synthesized using the $[Mo(CN)_7]^{4-}$ precursor, has been investigated.[9−13] In these networks (see the Supporting Information for structural details), the structure of the heptacyanomolybdate fragment was viewed either as a distorted pentagonal bipyramid[11,12,14,15] or as a distorted capped trigonal prism.[9,13,15] In these networks the spin $S = {}^1/_2$ of molybdenum sites is expected to be strongly anisotropic, giving rise to both single-ion anisotropy[9,11] and strong anisotropic exchange interactions in the Mo(III)−CN−Mn(II) pairs.[14] These contributions, together with the contributions from the magnetic dipolar interaction,[9,11] are the reason for the anisotropic magnetic behavior observed in all cyano-bridged networks, which is manifested as a strong orientation dependence of the magnetization, field-induced spin reorientation transitions, and unexpected ferromagnetic Curie−Weiss susceptibility.[9−13] All these aspects will be analyzed in a forthcoming publication.[16]

In the present article, we investigate the magnetic anisotropy of $[Mo(CN)_7]^{4-}$ for two ideal geometries of the pentagonal bipyramid (Figure 1a) and capped trigonal prism (Figure 1b) along with the heptacyanomolybdate fragment of the cyano-bridged magnetic network $K_2[Mn(H_2O)_2]_3[Mo(CN)_7]_2\cdot 6H_2O$ (Figure 2). To this end, we combine quantum chemistry calculations with the ligand field analysis and compare the calculated g tensors with available data from experiment. Our results show that the ligand field spectra of $[Mo(CN)_7]^{4-}$ anions

* E-mail: Liviu.Chibotaru@chem.kuleuven.ac.be.
† Katholieke Universiteit Leuven.
‡ Université Montpellier II.

10.1021/jp051858j CCC: $30.25
Published on Web 07/22/2005

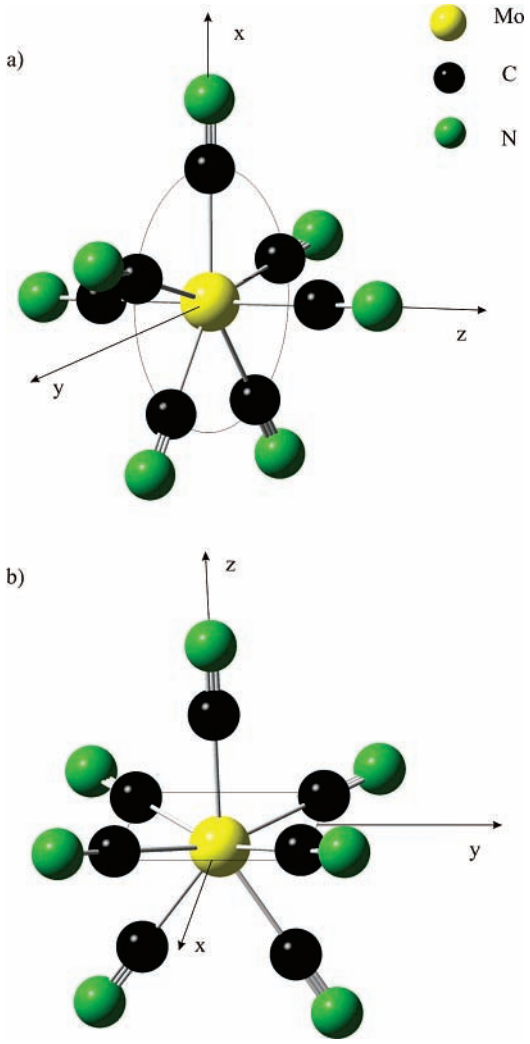

Figure 1. Pentagonal bipyramidal (a) and capped trigonal prismatic (b) coordination environment of the molybdenum site.

at different geometries have a low-lying excited state, which is the reason a significant magnetic anisotropy at molybdenum sites persists for variously distorted coordination environments in the fragments of Mo−Mn cyano-bridged networks. [9−13]

Computational Details

The electronic structure of the $[Mo(CN)_7]^{4-}$ complexes has been studied by an ab initio method. Due to the near-degeneracy effects arising from the ligand field splitting of the d orbitals, the CASPT2[19] method was chosen to calculate the excitation energies of the low-lying ligand field states. The active spaces employed in the CASSCF part of this computational technique consisted of the five d orbitals among which the three valence electrons of the metal cation are distributed. By using these CASSCF wave functions as a reference, the dynamic electron correlation was estimated by a multiconfigurational second-order perturbation approach. In this part of the CASPT2 calculations, all the valence electrons of the complex anion were taken into account, namely the 2s and 2p electrons of carbon and nitrogen and the 4s, 4p, and 4d electrons of molybdenum.

This computational approach has been proven in the past, by a similar CASPT2 study on the related $[Mo(CN)_8]^{4-}$, to be sufficient for obtaining a reliable description of the ligand field spectrum.[17] The molecular orbitals of the two complexes are expanded in an all-electron basis set for all the atoms of the complex. For the molybdenum cation an ANO basis set of the

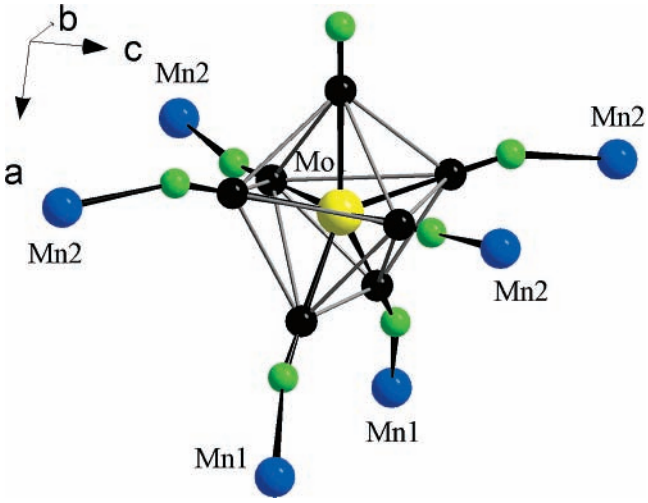

Figure 2. Local coordination environment of Mo site of $K_2[Mn(H_2O)_2]_3[Mo(CN)_7]_2{\cdot}6H_2O$.

type (21s, 17p, 12d, 5f)/[6s, 5p, 4d, 1f] was used,[18] whereas for carbon and nitrogen atoms the [3s, 2p, 1d] ANO-L basis sets as present in the library of the MOLCAS software package were chosen.[19] In crystals the $[Mo(CN)_7]^{4-}$ complex is frequently observed as a more or less distorted pentagonal bipyramid or capped trigonal prism. All the Mo−C and C−N bond distances of an idealized D_{5h} geometry of the pentagonal bipyramidal isomer were set equal to the average X-ray values of 2.151 and 1.154 Å, respectively.[11] Geometrical parameters for the capped trigonal prismatic isomer were taken from a recently published X-ray study of $K_2[Mn(H_2O)_2]_3[Mo(CN)_7]_2{\cdot}6H_2O$.[10] Within this isomer three types of cyanide ligands can be distinguished: one top cyanide, two wedge cyanides, and four cyanides located at the four corners of a square. The experimental bond distances and angles were averaged to obtain an idealized C_{2v} geometry. The Mo−C and C−N distances employed are: 2.185 and 1.144 Å for the top cyanide, 2.127 and 1.158 Å for the wedge cyanides, and 2.155 and 1.154 Å for the remaining four cyanides (square). C(top)−Mo−C (square) and C(top)−Mo−C (wedge) bond angles were set equal at 81° and 142°, respectively. In close agreement with the experimental structures, for both idealized geometries a bond angle of 180° was chosen for all Mo−C−N fragments. In addition to these two symmetric limits, additional calculations on the actual geometry of the $[Mo(CN)_7]^{4-}$ complex anion in $K_2[Mn(H_2O)_2]_3[Mo(CN)_7]_2{\cdot}6H_2O$ were carried out. CASPT2 total energies were calculated by taking into account scalar relativistic effects according to the Douglas−Kroll method,[20] whereas spin−orbital coupling effects were obtained by evaluating effective one-electron Hamiltonian matrix elements between CASSCF reference wave functions.[21]

Results and Discussion

Ligand Field Parameters. An analysis of our CASPT2 transition energies for various excitations of the *pentagonal bipyramid* isomer (Figure 1a) confirms the well-known electronic structure. The ground state is calculated to be a $^2E_1''$ state as a result of the occupation of the e_1'' shell (d_{xz} and d_{yz}, the z axis coinciding with the C_5 axis of the D_{5h} point group, Figure 1a) by three valence electrons. The lowest-lying quartet and doublet ligand field states arise from a single electron excitation to the higher-lying e_2' orbitals and are situated at energies higher than 24 000 cm^{-1}. Excitations to the highest-lying d_{z^2} (a_1') orbital are found at even higher energies. The spectrum of lowest ligand

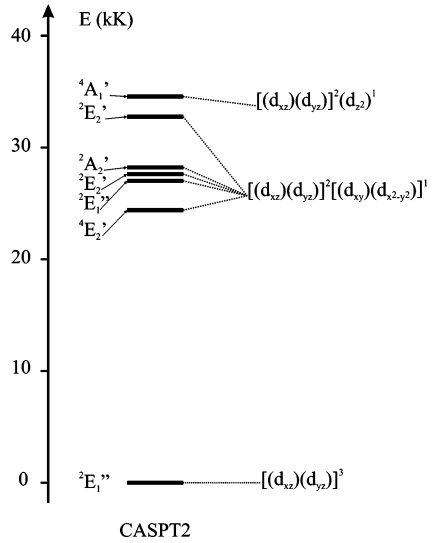

Figure 3. Lowest ligand field terms of pentagonal bipyramidal complex $Mo(CN)_7^{4-}$.

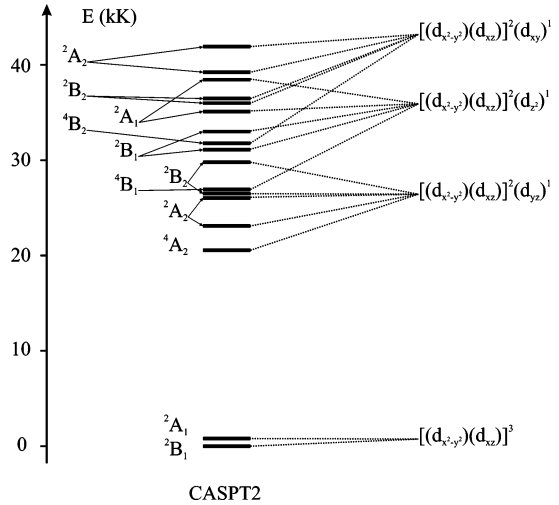

Figure 4. Lowest ligand field terms of capped trigonal prismatic complex $Mo(CN)_7^{4-}$.

field levels is shown in Figure 3. A fitting of the CASPT2 transition energies (Table 1S in Supporting Information) to ligand field expressions yields the following ligand field and Racah parameters: $e_\sigma = 25\,850$ cm^{-1}, $e_\pi = 9100$ cm^{-1}, $B = 290$ cm^{-1}, and $C = 1150$ cm^{-1}. These values agree very well with the results obtained recently for $[Mo(CN)_6]^{3-}$ by using the same computational approach.[22] Due to spin−orbit coupling the ground state is found to split into two Kramers doublets. The zero-field splitting between them amounts to 489 cm^{-1}, which is therefore our calculated value for the spin−orbit coupling constant ζ.

For the second geometry of $[Mo(CN)_7]^{4-}$, the *capped trigonal prism* (Figure 1b), the electronic structure is slightly more complicated and therefore less well understood in the literature. The calculated spectrum of lowest ligand field levels is shown in Figure 4. From an analysis of the CASSCF reference wave functions of the low-lying ligand field states and their relative energies, we deduced the following orbital splitting scheme. When placing the top cyanide on the *z* axis, the four square cyanides between the *x* and *y* directions and the two wedge cyanides in the *yz* plane (Figure 6), we calculate the d_{xz} and $d_{x^2-y^2}$ orbitals as the lowest ones. They are, however, nearly degenerate, as is reflected by the fact that the two resulting

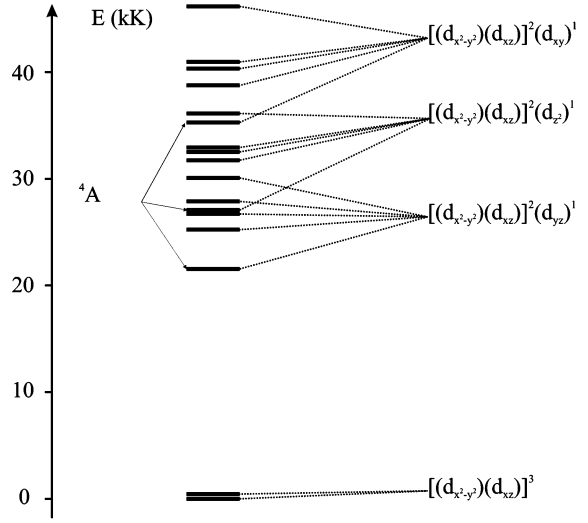

Figure 5. Lowest ligand field terms of $Mo(CN)_7^{4-}$ fragment of $K_2[Mn(H_2O)_2]_3[Mo(CN)_7]_2 \cdot 6H_2O$.

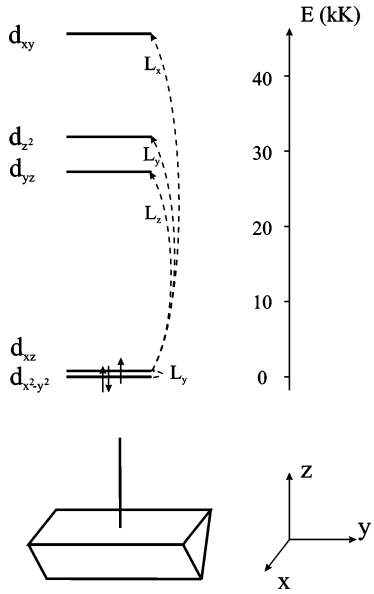

Figure 6. Single-electron excitations in the capped trigonal prismatic complex $Mo(CN)_7^{4-}$ from the ground electronic configuration $(d_{x^2-y^2})^2(d_{xz})^1$ shown by dashed arrows. The component of the orbital momentum that can admix for each transition is indicated in the right-hand side of the energy diagram.

doublet states are quite close in energy. At the CASPT2 level, the ground state turns out to be a $^2B_1$ $((d_{xz})^1(d_{x^2-y^2})^2)$ while the energy difference with the $^2A_1$ $((d_{xz})^2(d_{x^2-y^2})^1)$ amounts only to 803 cm^{-1}. After incorporating spin−orbit coupling this energy gap is slightly raised to 854 cm^{-1}, which implies a spin−orbit coupling constant ζ of 317 cm^{-1}. The smaller value of this constant as compared to the value calculated for the pentagonal bipyramid reflects the more covalent character of the $d_{x^2-y^2}$ orbital. Indeed, in the capped trigonal prismatic isomer this orbital has a substantial σ-type interaction with the two wedge cyanides. Other excited states are located at energies higher than 20 000 cm^{-1}. Fitting the transition energies (Table 2S in Supporting Information) to ligand field expressions yields parameters that resemble quite well the values obtained for the pentagonal bipyramid: $e_\sigma = 25\,300$ cm^{-1}, $e_\pi = 8200$ cm^{-1}, $B = 230$ cm^{-1}, and $C = 900$ cm^{-1}. To achieve the correct order of the lowest two states, $^2B_1$ and $^2A_1$ mentioned above, a

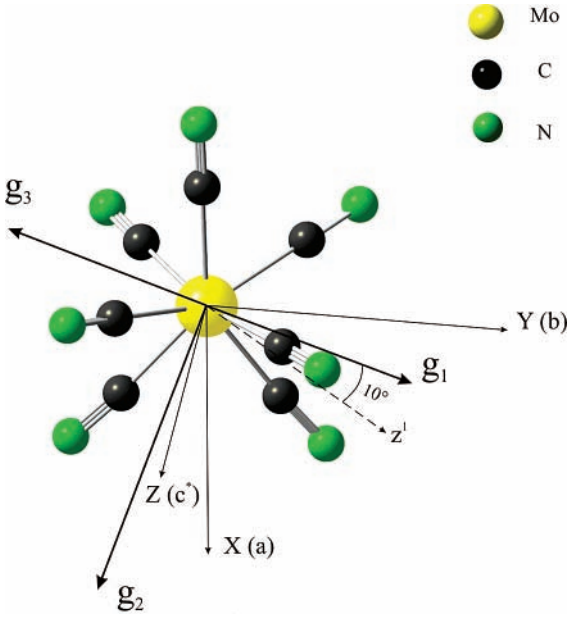

Figure 7. $Mo(CN)_7^{4-}$ fragment of $K_2[Mn(H_2O)_2]_3[Mo(CN)_7]_2 \cdot 6H_2O$ relative to the magnetic axes of the crystal *abc**. The axes g_1, g_2, and g_3 are the principal magnetic axes of the fragment. z^1 shows the direction of the main symmetry axis of the pentagonal bipyramid (cf. Figure 1).

different Racah parameter A for the lowest d orbitals is needed: $\Delta A_{xz} = 829\ cm^{-1}$ and $\Delta A_{x^2-y^2} = -3922\ cm^{-1}$. The obtained smaller A for $d_{x^2-y^2}$ reflects a stronger covalency of this orbital as compared to that of d_{xz}.

The excitation energies calculated for the *actual geometry of the* $[Mo(CN)_7]^{4-}$ fragment in $K_2[Mn(H_2O)_2]_3[Mo(CN)_7]_2 \cdot 6H_2O$ (Figure 2, Figures 1S−3S in Supporting Information) resemble to a large extent the ones obtained for the capped trigonal prism. The splitting between the two lowest states is reduced to 318 cm^{-1} at the CASPT2 level of calculation (Figure 5, Table 3S in Supporting Information). These states mainly correspond to the configurations $(d_1)^2(d_2)^1$ (ground) and $(d_1)^1(d_2)^2$ (excited). The frontier d orbitals have the following form in the coordinate system related to the magnetic axes of the crystal *abc** (Figure 7):

$$d_1 \approx 0.82d_{xz} - 0.43d_{x^2-y^2} + 0.35d_{xy}$$
$$d_2 \approx 0.75d_{z^2} + 0.54d_{x^2-y^2} + 0.39d_{xz} \qquad (1)$$

The gap between the ground and the first excited state is raised to 447 cm^{-1} when the spin−orbit coupling is included, from which we derived $\zeta = 310\ cm^{-1}$. Next excited states are located at energies >19 300 cm^{-1} (Figure 5). The best fit of the ligand field energies to the CASPT2 transition energies (Table 3S in Supporting Information) is achieved for the following ligand field and Racah parameters: $e_\sigma = 25\,400\ cm^{-1}$, $e_\pi = 7500\ cm^{-1}$, $B = 220\ cm^{-1}$, and $C = 900\ cm^{-1}$. As in the case of capped trigonal prismatic geometry, to fine-tune the relative energies of the lowest two states a correction to the Racah parameter A corresponding to the orbital d_{z^2} was introduced, $\Delta A_{z^2} = -1460\ cm^{-1}$.[23]

Calculation of the *g* Tensors. The obtained ligand field parameters have been used for the calculation of the g tensor of $[Mo(CN)_7]^{4-}$ in the three geometries (Table 1). To this end, the Zeeman interaction has been introduced:

$$H_{Zee} = \mu_B \sum_i (g_e \vec{s}^{\,i} + k\vec{l}^{\,i})\vec{H} \qquad (2)$$

TABLE 1: *g* Tensors of $Mo(CN)_7^{4-}$ Complexes in Different Geometries

PBP (D_{5h})	CTP (C_{2v})	$K_2[Mn(H_2O)_2]_3[Mo(CN)_7]_2 \cdot 6H_2O$ fragment (C_1)
$g_{\|\|} = 3.20$	$g_y = 2.23$	$g_1 = 2.53$
$g_\perp \approx 0.00$	$g_x = 1.88$	$g_2 = 1.41$
$\zeta = 489\ cm^{-1}$	$g_z = 1.87$	$g_3 = 1.39$
$k = 0.60$	$\zeta = 317\ cm^{-1}$	$\zeta = 310\ cm^{-1}$
	$k = 0.39$	$k = 0.38$

where the sum runs over the molybdenum 4d electrons, s and l are electron spin and orbital operators, respectively, H is the applied magnetic field, and k is the orbital reduction factor. The elements of the g tensor have been extracted from the Zeeman splittings of the lowest Kramers doublet for different orientations of the applied magnetic field. The orbital reduction factor k entering eq 2 has been estimated as the ratio of the spin−orbit constant ζ at a given geometry (Table 1) to the spin−orbit constant in a free ion Mo^{3+}, $\zeta_{ion} = 817\ cm^{-1}$.[24] The resulting orbital reduction factors for each geometry are listed in the last row of Table 1.

The g tensor of pentagonal bipyramidal complex is axial as expected and very anisotropic. The obtained high magnetic anisotropy is the result of the joint effect of fivefold axial symmetry with a large crystal field gap to the excited orbitals. The degenerate ground electronic configurations, $(d_{xz})^2(d_{yz})^1$ and $(d_{yz})^2(d_{xz})^1$, are split by spin−orbit interaction into two Kramers doublets. The components of the ground doublet are described by the configurations $(d_{+1})^2(d_{-1})^{\uparrow}$ and $(d_{-1})^2(d_{+1})^{\downarrow}$. Here the new orbitals $d \pm 1 = (d_{xz} \pm id_{yz})/\sqrt{2}$ have definite values of the projection of orbital momentum (± 1) on the z axis of the pentagonal bipyramid (Figure 1), and the arrows in the superscripts denote the spin projection on the same axis. These configurations differ by one orbital and one spin projection and therefore cannot be mixed by the Zeeman interaction. As a result, no magnetic moments can be induced in the equatorial plane, and we have for the corresponding component of the g tensor: $g_\perp = 0$. The Zeeman energies of the two components of the Kramers doublet are $\pm\mu_B(^1/_2 g_e + k)H_z$, which for $k = 0.6$ gives for $g_{||}$ the value 3.2 as seen in Table 1. Note that we derive the effect of Zeeman interaction on the spin−orbital states, that is, with spin−orbit coupling already included, and therefore the excited terms (e.g., the first excited Kramers doublet) will admix only in the second order after the Zeeman term and hence will not contribute to the g tensor. On the other hand, the excited configurations can admix to the ground one via the electron repulsion in the d shell (multiplet effects), which results in a nonzero value of $g_\perp$. As ligand field calculations show, this effect is very small because of large crystal field gaps to the excited configurations. The negligible admixture of these configurations can be also seen in CASSCF results, which show 99% weight of the ground configuration in the ground state. Despite this clear picture, the obtained results differ much from the measured ESR g tensor components of the complex $NaK_3[Mo(CN)_7] \cdot 2H_2O$,[8] claimed to be close to a pentagonal bipyramid, for which the values $g_{||} = 3.89$, $g_\perp = 1.77$ have been obtained. We can suggest that these g components result from the deviations of the actual geometry of the complex from an ideal pentagonal bipyramidal geometry. Such deviations are seen indeed in the X-ray data of the compound; however, the published structural data in ref 8 is not detailed enough for a quantum chemistry calculation. Further structural investigations are clearly necessary to settle this controversy.

The g tensor of a capped trigonal prismatic complex (second column in Table 1) is far less anisotropic than the pentagonal

bipyramidal one, which is obviously due to its lower C_{2v} symmetry. This symmetry requires one axis of the *g* tensor to coincide with the C_2 rotational axis and the other two to lie on the mirror planes σ_v and σ_v'. The corresponding coordinate axes are *z*, *x*, and *y*, respectively, in Figure 6. Table 1 shows that the *g* tensor is close to an axial one, which is not expected in the C_{2v} geometry. To understand this we first examine the admixture of excited configurations to the ground one, $(d_{x^2-y^2})^2(d_{xz})^1$, by different components of the orbital momentum. Only four excited configurations contribute to the *g* tensor in the first order after spin−orbit coupling as shown in Figure 6,[25] which give the following conventional expressions[26] for the *g* components:

$$g_y = g_e + \frac{2k\zeta}{\Delta E_{(x^2-y^2\rightarrow xz)}} - \frac{6\zeta}{\Delta E_{(xz\rightarrow z^2)}}$$

$$g_x = g_e - \frac{2k\zeta}{\Delta E_{(xz\rightarrow xy)}}, \quad g_z = g_e - \frac{2k\zeta}{\Delta E_{(xz\rightarrow yz)}} \qquad (3)$$

Taking *k* and ζ from the second column of Table 1 and the excitation energies from Figure 6, we obtain with these equations $g_y = 2.284$, $g_x = 1.994$, $g_z = 1.991$.

While the anisotropy in the *y* direction is reproduced correctly by eq 3 (the larger value of g_y is obviously due to the small excitation energy $\Delta E(x^2 - y^2 \rightarrow xz)$), the orbital corrections to g_x and g_z are too small (cf. the results in Table 1). The reason is a relatively large spin−orbit coupling compared to the energy gap between the lowest states, which makes the first-order perturbation theory after ζ insufficient for the correct treatment of the *g* tensor. We show this by an exact treatment of the effect of spin−orbit coupling on the lowest two configurations. According to Figure 6, for these states the only nonzero matrix elements of the spin−orbit operator are $\langle d_{xz}\uparrow d_{x^2-y^2}\uparrow | \sum_i \xi(r_i)\, l_y^i s_y^i | d_{xz}\uparrow d_{xz}\downarrow d_{x^2-y^2}\downarrow\rangle = \zeta/2$ and a similar one for opposite spin projections, which gives rise to the following matrix for the two Kramers doublets:

$$\hat{H} = \begin{pmatrix} 0 & \zeta/2 \\ \zeta/2 & \Delta \end{pmatrix} \qquad (4)$$

where the notation $\Delta \equiv \Delta E(x^2 - y^2 \rightarrow xz)$ was introduced. Diagonalizing this matrix gives the solution for the lowest Kramers doublet:

$$|\Gamma_\alpha\rangle = \sqrt{1-c^2}\,|d_{xz}\uparrow d_{x^2-y^2}\downarrow d_{x^2-y^2}\downarrow| + c\,|d_{xz}\uparrow d_{xz}\downarrow d_{x^2-y^2}\downarrow|$$

$$|\Gamma_\beta\rangle = \sqrt{1-c^2}\,|d_{xz}\downarrow d_{x^2-y^2}\uparrow d_{x^2-y^2}\downarrow| + c\,|d_{xz}\uparrow d_{xz}\downarrow d_{x^2-y^2}\uparrow| \qquad (5)$$

A straightforward calculation of the matrix elements of the Zeeman operator (eq 2) with these wave functions gives the following expressions for the *g* components:

$$g_x = g_z = g_e(1 - 2c^2)$$

$$g_y = g_e - 4kc\sqrt{1-c^2} \qquad (6)$$

In the first-order approximation we have for the lowest solution of (eq 4) $c = -\zeta/2\Delta \approx -0.2$. Substituting this into eq 6 gives values of the *g* components that reproduce well the results in Table 1. We may draw two conclusions from this analysis. First, we observe from eq 5 that the spin−orbit coupling admixes configurations of opposite spin to each component of the Kramers doublet. This leads to a reduction of the spin moments in these states ($\pm^1/_2$) by the factor $(1 - 2c^2)$. Since the orbital momentum is quenched in the *x* and *z* directions (Figure 6), the corresponding components of the *g* tensor are the free spin value g_e multiplied by this factor. Note that these corrections to the *g* tensor are of the order $c^2 \approx \zeta^2/\Delta^2$, which is a *second-order effect* after spin−orbit coupling. Second, the axial form of the *g* tensor emerges automatically because the orbital momentum gives nonzero contribution only in one direction (*y*). The orthorhombic symmetry of the *g* tensor is restored by the admixture of other excited states (Figure 6) but the resulting corrections are small as discussed above.

The obtained *g* components are in reasonable agreement with experimental ones derived from ESR spectrum of $K_4Mo(CN)_7 \cdot 2H_2O$: $g_{\|} = 2.103$, $g_{\perp} = 1.973$.[6] We find, however, that the anisotropy axis ($g_{\|}$) is not oriented along the symmetry axis of the complex (*z* in Figure 6) but in a different direction (*y*). This is an example of strong orbital symmetry control of the *g* factor anisotropy, found also for other low-symmetry complexes,[27] which is entirely defined by the lowest ligand field orbitals. Indeed, earlier ligand field simulations for this compound in ref 6 gave the order of orbitals $\epsilon(d_{xy}) < \epsilon(d_{x^2-y^2}) < \epsilon(d_{yz}) < \epsilon(d_{xz}) < \epsilon(d_{z^2})$, yielding in particular the ground configuration $(d_{xy})^2(d_{x^2-y^2})^1$, which differs substantially from single-electron excitations in Figure 6. As a result, the authors of ref 6 came to a different assignment of the *g* components: $g_{\|} = g_z$, $g_{\perp} = g_x \approx g_y$. One should stress that the present results are obtained by a rigorous ab initio method. Moreover, the order of one-electron excitations in Figure 6 cannot be reproduced by any ligand field parameters e_σ and e_π without introducing orbital-specific corrections to the Racah parameters. Such corrections could not be anticipated within the ligand field approach alone.

Finally, the *g* tensor for the $Mo(CN)_7^{4-}$ fragment of $K_2[Mn(H_2O)_2]_3[Mo(CN)_7]_2 \cdot 6H_2O$ (Figure 7) is expected to be of a general form according to the C_1 symmetry of this fragment. In the *XYZ* coordinates related to the magnetic axes of the crystal it is obtained as follows:

$$g = \begin{array}{c} \begin{matrix} X & Y & Z \end{matrix} \\ \begin{pmatrix} 1.44 & -0.17 & -0.12 \\ & 2.07 & 0.53 \\ & & 1.82 \end{pmatrix} \end{array} \qquad (7)$$

Diagonalization of eq 7 gives the main values of the *g* tensor as shown in the last column of Table 1, and the local magnetic axes which are oriented relative to *abc** as shown in Figure 7. One can deduce from Table 1 that the *g* tensor is again of the axial form. The reason for that is the same as in the case of capped trigonal prism: the small energy gap between the ground and the first excited configuration (318 cm^{-1} in the present case). Indeed, due to the small value of this gap we can again confine ourselves to the two lowest electronic configurations, $(d_1)^2(d_2)^1$ and $(d_1)^1(d_2)^2$, where the orbitals d_1 and d_2 are defined in eq 1. Now, it is well-known that any two real d orbitals defined in a canonical way are connected by only one Cartesian component of the orbital momentum and have zero matrix elements for another two components (see, for example, Appendix 2 in ref 3). This is easily generalized over any pair of real orbitals d_1 and d_2: we always can find such directions for the new Cartesian axes (123) that $\langle d_1|L_1|d_2\rangle \neq 0$, $\langle d_1|L_2|d_2\rangle = \langle d_1|L_3|d_2\rangle = 0$.[28] Then the results obtained above for the *g* tensor of capped trigonal prism, eqs 4−6, are equally applicable to the present case. We merely need to relabel in these equations the Cartesian axes *x*, *y*, and *z* by 2, 1, and 3, respectively, and replace the orbitals $d_{x^2-y^2}$ and d_{xz} by d_1 and d_2, respectively. The only modification is the coefficient in front of ζ in eq 4, which is different from $^1/_2$ for arbitrary orbitals d_1 and d_2. Accordingly,

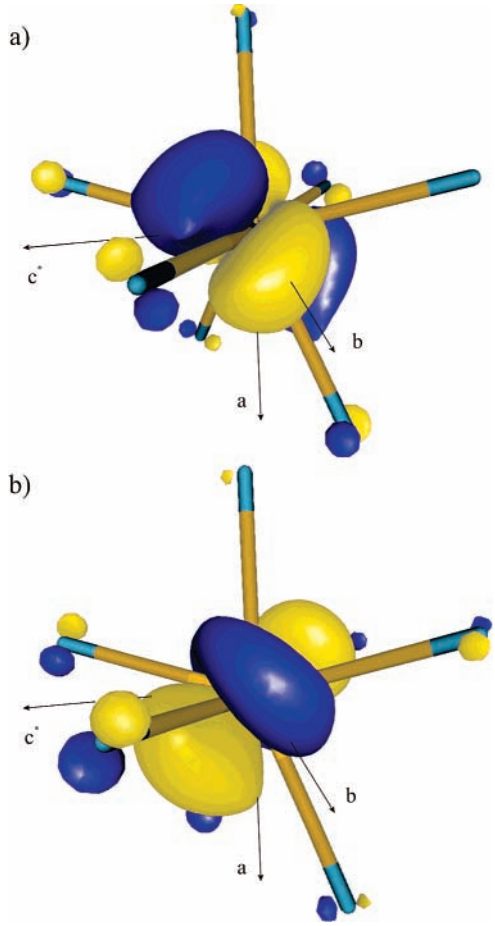

Figure 8. Doubly occupied (a) and singly occupied (b) molybdenum orbitals of 4d type in the $Mo(CN)_7^{4-}$ fragment of $K_2[Mn(H_2O)_2]_3[Mo(CN)_7]_2 \cdot 6H_2O$. Their states correspond approximately to d_1 and d_2 in eq 1, respectively.

the axial component of the *g* tensor (g_1 in Table 1) is related to the axis 1 defined above.

The stronger magnetic anisotropy in the investigated $Mo(CN)_7$ fragment ($g_\perp/g_\parallel \approx {}^1/_2$) compared to the capped trigonal prism is due to the lower value of the gap Δ in the former case, which leads to a higher absolute value of the coefficient *c* in eq 6.[30] Moreover, as Figure 7 shows, the obtained anisotropy axis (the axis 1) makes only 10° with the symmetry axis z^1 of the pentagonal bipyramid (axis *z* in Figure 1a). All this reflects the intermediate structure of the fragment, which is between pentagonal bipyramidal and trigonal prismatic geometry. Figure 8 shows the occupied orbitals d_1 and d_2 of the ground configuration. The doubly occupied one (d_1) looks very similar to one of the lowest orbitals (d_{xz} or d_{yz}) in the pentagonal bipyramidal complex (the directions of the Mo−CN bonds passing between *b* and *c** in Figure 8 are close to the symmetry axis z^1 of pentagonal bipyramid). The orbital d_2 cannot be viewed, however, as a merely rotated d_1 around the axis z^1 by 90° (Figure 8b). Its shape is determined by additional contributions from other 4d orbitals as a consequence of the deviation of the geometry from a pentagonal bipyramid.

The main structural transformation accompanying the transition from capped trigonal prismatic to pentagonal bipyramidal geometry is the rotation of the plane of two wedge cyanides from the *XY* coordinate plane (Figure 7) to a plane bisecting the *XZ* and *XY* coordinate planes, that is, by 45°. We can infer from our calculations that in the course of this transformation the gap between the lowest electronic states (Δ) will gradually decrease from its maximal value in capped trigonal prism (800 cm^{-1}) to zero in pentagonal bipyramid. This transition is accompanied by a gradual increase of magnetic anisotropy, as follows from eq 6, while the *g* tensor will always remain axial. Concomitantly, the anisotropy axis will rotate from the axis *Y* (Figure 7) to the axis *z*.[1] The magnetic anisotropy is found to be quite strong in the $Mo(CN)_7^{4-}$ fragment of $K_2[Mn(H_2O)_2]_3[Mo(CN)_7]_2 \cdot 6H_2O$, with the anisotropy axis close to z^1. This is a remarkable result because the structure of this fragment was found in the symmetry analysis to be closer to capped trigonal prism than to pentagonal bipyramid.[15] We may expect that $Mo(CN)_7^{4-}$ fragments in other Mo(III)−Mn(II) cyano-bridged networks are even more anisotropic because their structures are closer to a pentagonal bipyramid than its structure in $K_2[Mn(H_2O)_2]_3[Mo(CN)_7]_2 \cdot 6H_2O$.

Conclusions

The specific feature of heptacyano Mo(III) complexes is the presence of a low-lying excited state, separated from the ground state by only several hundred wavenumbers. This is the reason for the axial form of the *g* tensor and strong magnetic anisotropy of $[Mo(CN)_7]^{4-}$ units even at strongly distorted geometries of the corresponding fragments in cyano-bridged networks. Ab initio and ligand field calculations of the *g* tensor of molybdenum sites in $K_2[Mn(H_2O)_2]_3[Mo(CN)_7]_2 \cdot 6H_2O$ show that the principal magnetic axes deviate significantly from the magnetic axes of this crystal and the magnetic anisotropy of molybdenum sites is quite strong $g_\perp/g_\parallel \approx {}^1/_2$. This allows us to assume that the unusual manifestation of magnetic anistropy in cyano-bridged networks based on $[Mo(CN)_7]^{4-}$ is probably because the magnetic properties of heptacyano Mo(III) fragments remain close to those of a pentagonal bipyramid.

Acknowledgment. Financial support from the Belgian Science Foundation and Flemish Government under the Concerted Action Scheme, the INTAS Grant 00-00565, the CNRS (France), and the University of Montpellier II is gratefully acknowledged. We thank Dr. Eliseo Ruiz for the symmetry analysis of the local Mo environment.

Supporting Information Available: Crystallographic data on the crystal $K_2[Mn(H_2O)_2]_3[Mo(CN)_7]_2 \cdot 6H_2O$[12]. This material is available free of charge via the Internet at http://pubs.acs.org.

References and Notes

(1) (a) Boyd, P. D. W.; Li, Q.; Vincent, J. B.; Folting, K.; Chang, H. R.; Streib, W. E.; Huffman, J. C.; Christou, G.; Hendrickson, D. *J. Am. Chem. Soc.* **1988**, *110*, 8537−8539. (b) Caneschi, A.; Gatteschi, D.; Sessoli, R.; Barra, A. L.; Brunel, L. C.; Guillot, M. *J. Am. Chem. Soc.* **1991**, *113*, 5873−5874. (c) Sessoli, R.; Gatteschi, D.; Caneschi, A.; Novak, M. *Nature* **1993**, *365*, 141−143. (d) Sessoli, R.; Tsai, H. L.; Schake, A. R.; Wang, S.; Vincent, J. B.; Folting, K.; Gatteschi, D.; Christou, G.; Hendrickson, D. *J. Am. Chem. Soc.* **1993**, *115*, 1804−1816. (e) Awschalom, D. D.; Di Vincenzo, D. P. *Phys. Today* **1995**, *48*, 43. (f) Dahlberg, E. D.; Zhu, J.-G. *Phys. Today* **1995**, *48*, 34−41.

(2) Gatteschi, D.; Sorace, L. *J. Solid State Chem.* **2001**, *159*, 253−261.

(3) Kahn, O. *Molecular Magnetism*; VCH Publishers: New York, 1993.

(4) Bencini, A.; Gatteschi, D. *EPR of Exchange Coupled Systems*; Springer-Verlag: Berlin, 1990.

(5) Moria, T. In *Magnetism*; Rado, G. T., Suhl, H., Eds.; Academic Press: New York, 1963.

(6) Rossman, R. G.; Tsay, F. D.; Gray, H. B. *Inorg. Chem.* **1973**, *12*, 824−829.

(7) Drew, M. G. B.; Mitchell, P. C. H.; Pygal, C. E. *J. Chem. Soc., Dalton* Trans. **1977**, 1071−1077.

(8) Hursthouse, M. B.; Malik, K. M. A.; Soares, A. M.; Gibson, J. F.; Griffith, W. P. *Inorg. Chim. Acta* **1980**, *45*, L81−L82.

(9) Kahn, O.; Larionova, J.; Quahab, L. *Chem. Commun.* **1999**, 945−952.

(10) Larionova, J.; Willemin, S.; Donnadieu, B.; Henner, B.; Guérin, C.; Gillon, B.; Goujon, A. *J. Phys. Chem. Solids* **2004**, *65*, 677−691.

(11) (a) Larionova, J.; Kahn, O.; Golhen, S.; Quahab, L.; Clérac, R. *Inorg. Chem.* **1998**, *38*, 3621−3627. (b) Larionova, J.; Clérac, R.; Sanchiz, J.; Kahn, O.; Golhen, S.; Quahab, L. *J. Am. Chem. Soc.* **1998**, *120*, 13088−13095.

(12) (a) Larionova, J.; Kahn, O.; Golhen, S.; Quahab, L.; Clérac, R. *J. Am. Chem. Soc.* **1999**, *121*, 3349−3356. (b) Le Goff, X. F.; Clérac, R.; Coulon, C.; Donnadieu, B. *J. Phys. IV* **2004**, 633−636.

(13) (a) Willemin, S.; Le Goff, X. F.; Donnadieu, B.; Clérac, R.; Guérin, Ch.; Henner, B.; Larionova, J., to be submitted for publication. (b) Larionova, J.; Clérac, R.; Donnadieu, B.; Guérin, Ch. *Chem.−Eur. J.* **2002**, *8*, 2712.

(14) Mironov, V. S.; Chibotaru, L. F.; Ceulemans, A. *J. Am. Chem. Soc.* **2003**, *125*, 9750−9760.

(15) The symmetry analysis of the local coordination environment of Mo sites in $K_2[Mn(H_2O)_2]_3[Mo(CN)_7]_2{\cdot}6H_2O$ was performed by Dr. Eliseo Ruiz (Electronic Structure Group, Universitat de Barcelona, Spain) using the program Shape V1.1a (Continuous Shape Measures Calculations). Five models were considered: heptagon (D_{7h}), hexagonal pyramid (C_{6v}), pentagonal bipyramid, capped octahedron (C_{3v}), and capped trigonal prism. The obtained results show that the most probable geometry corresponds to the capped trigonal prism. The capped octahedral geometry was also found as a possible local environment, but with lesser probability. (Willemin, S.; Larionova, J.; Bolvin, H.; Donnadieu, B.; Le Goff, X. F.; Ruiz, E.; Guerin, Ch.; Henner, B. *Polyhedron* **2005**, *24*, 1033−1046.)

(16) Chibotaru, L. F.; Larionova, J.; Hendrickx, M. F. A.; Clima, S.; Ceulemans A. Katholieke Universiteit Leuven, Belgium, to be submitted for publication.

(17) Hendrickx, M. F. A.; Mironov, V. S.; Chibotaru, L. F.; Ceulemans A. *Inorg. Chem.* **2004**, *43*, 3142−3150.

(18) RCC basis set for molybdenum is available in *MOLCAS 6.0*.

(19) *MOLCAS*, version 6.0; Karlström, G.; Lindh, R.; Malmqvist, P.-Å.; Roos, B. O.; Ryde, U.; Veryazov, V.; Widmark, P.-O.; Cossi, M.; Schimmelpfennig, B.; Neogrady, P.; Seijo, L. *Comput. Mater. Sci.* **2003**, *28*, 222.

(20) Douglas N.; Kroll N. M. *Ann. Phys.* **1974**, *82*, 89.

(21) Malmqvist, P. A.; Roos, B. O.; Schimmelpfennig, B. *Chem. Phys. Lett.* **2002**, *357*, 230−240.

(22) Hendrickx, M. F. A.; Mironov, V. S.; Chibotaru, L. F.; Ceulemans A. *J. Am. Chem. Soc.* **2003**, *125*, 3694−3695.

(23) Obviously this tuning is arbitrary: we could reproduce the gap between the lowest doublets by introducing corrections to the Racah parameter A corresponding to either d_{xz} and/or $d_{x^2-y^2}$ orbitals. We note, however, that this does not influence further results since the composition of the lowest orbitals d_1 and d_2, eq 1, is not sensitive to the tuning procedure.

(24) Griffith, J. S. *The Theory of Transition-Metal Ions*; Cambridge University Press: Cambridge, 1971.

(25) As in the case of pentagonal bipyramid, we disregard the admixture of excited configurations via electron repulsion for similar reasons.

(26) Abragam, A.; Bleaney, B. *Electron Paramagnetic Resonance of Transition Ions*; Clarendon Press: Oxford, 1970.

(27) Ceulemans, A.; Debuyst, R.; Dejehet, F.; King, G. S. D.; Vanhecke, M.; Vanquickenborne, L. G. *J. Phys. Chem.* **1990**, *94*, 105−113.

(28) Indeed, the rotation of Cartesian coordinate system is described by three independent parameters, the Euler angles φ, θ, ψ (see, for example, ref 29), while only two conditions (zero matrix elements of L_2 and L_3) are to be satisfied.

(29) Landau, L. D.; Lifshitz, E. M. *Quantum Mechanics*, 2nd ed.; Pergamon Press: Oxford, 1975.

(30) In the limit of vanishing Δ we obtain $c = -1/\sqrt{2}$ and eq 6 recovers the result for the pentagonal bipyramid: $g_y = g_e + 2k$, $g_x = g_z = 0$.